Depth-of-Interaction Resolution Improvement due to Directional Control of Scintillator Light

Somya Pathak

Positron emission tomography (PET) uses radioactive tracers to localize disease manifestation in the body by mapping the gamma rays the tracers emit. PET scans are essentially maps of the varying levels of radiation inside the body in real space and time. Arrays of crystals called scintillators detect the position of the gamma ray's interaction—this point of interaction is different from the gamma ray's point of entry in that it is where the ray converts its energy into visible light. The interaction coordinates of the rays are uncertain without an accurate depth of interaction (DOI) value—a better accuracy, or resolution, of which allows for precise image reconstruction. Low DOI resolution leads to low spatial resolution as inaccurate positioning of the gamma events causes distortion of the final image. The pattern of visible light shared changes in accordance with the DOI. This light distribution is dependent on the path the light takes throughout the crystal. A portion of the light undergoes total internal reflection (TIR). Surface roughening can decrease TIR. Uniform depolishing, or roughening, is a process that involves mechanically or chemically treating the crystal's outer surfaces so they are no longer smooth. Here, a combination of polished and roughened sides are used in conjunction with a uniform light guide on top of the scintillator array improve DOI resolution at all module locations by optimizing the amount of TIR. Roughening the surface ensures light is scattered at a random angle, thus decreasing TIR. These light sharing patterns that are a function of DOI can be used to predict energy, timing, and spatial resolutions—all critical parameters of PET efficiency—of different PET modules. Varying the ratio of polished to roughened surfaces on Monte Carlo simulated scintillator sidewalls resulted in a wider range of light sharing values—this can be extrapolated to better DOI resolution. Simulated flood histograms showed improved crystal separation due to increased light output. Additionally, as a result of favorable surface roughening, the light sharing is more confined.

Introduction:

Low spatial resolution limits PET's ability to clearly outline the boundaries and location of small tumors. In fact, detection of tumors by clinical whole-body scanners is only reliable when the tumor is at least 7-10 mm (Avril and Adler, 2007). Limitations in current technology restrict the accuracy and the ability to visualize small tumors. Malignant cancer cells "have higher rates of aerobic glycolysis than other tissues" (Warburg, 1930)—they utilize more glucose than cells in normal cancer-free tissues. If a liquid solution composed of glucose bound to a radioisotope (this conjunction is known as a tracer) is injected into the bloodstream, the malignant cells will consume the injected glucose much more rapidly. Namely, the hungrier cancer cells will siphon more glucose than normal cells and because those molecules are tagged with nuclides emitting radiation, the malignant regions will also be radiation hotspots. These isotopes emit gamma rays that are detected by a PET scanner, which structurally is a ring of small detectors placed externally around the region of interest in the patient's body. These detectors can identify the origin point of the gamma rays. The more cancer cells will amount to increased amounts of tracer uptake which in turn corresponds to higher radiation at the location of the cancer cells.

PET is a diagnostic tool that provides functional body imaging through spatial and temporal maps of metabolic activity. The distribution of metabolic activity is represented by the distribution in radionuclide concentration. Radionuclides, or unstable atoms, specifically those so due to excess protons undergo positron decay (Penn et al., 2015). A proton converts into a neutron and a positron and a neutrino are released at the same time. Their emission is exclusive to the decay process—meaning the two particles do not pre-exist in the nucleus. Decreasing the nucleus' excess positive charge is a high priority. Neutrons are slightly bigger than protons. So, when a positron is emitted, the proton gains some mass but loses charge - because a positron has the same mass as an electron but opposite charge; it effectively becomes a neutron. While the neutrino does importantly help preserve angular momentum because its mass is so small and its net charge is zero, it does not affect the basics of beta decay. The emitted positron on the other hand lessens net positive charge, which stabilizes the nucleus by helping the atom achieve its most energetically favorable state possible. An unstable atom has excessive nuclear binding energy resulting from unbalanced forces. The strong forces in unstable atoms cannot generate enough binding energy to hold the nucleus together permanently. The positrons with their finite amount of energy slow down as they travel a very short distance through body matter and collide with electrons from the body matter's atoms in annihilation events. This path is so short and tortuous because the positron is constantly losing energy via ionization by neighboring atoms. An annihilation event produces two gamma rays of 511 keV (rest-mass equivalent of each particle; $E = mc^2$) that shoot away from each other in opposite directions. These rays can easily escape the body where they will be detected by the external PET scanner. In other

words, the positron and the electron—particles with equivalent mass but opposite charge—cancel each other out, leaving behind two massless high-energy gamma rays. Because the total momentum of the positron-electron system is zero just before their annihilation, the momentum of the resultant gamma rays must be such that momentum is conserved—this restriction helps deduce the gamma rays' exact energy. It is important to recognize that the actual location of the annihilation event is not recorded, only when each gamma ray reaches the detector and how much energy it deposits. Because of their antiparallel paths from the annihilation event, the pair of gamma rays travel along the same line of response (LOR). In a patient being administered a PET scan, thousands of these events will occur and therefore thousands of these LORs will be made. Regions of interest in the patient's body are where many of the LORs intersect; the more intersections, the more radiotracer indicated. Accurate localization of these events along the LOR is critical because they correspond to where the radiotracer has aggregated.

A PET scanner consists of a ring of modules whose position in relation to one another allows for the capture of both parts of the gamma ray pairs; it is placed externally around the patient. Each module is composed of an array of scintillator crystals coupled to a set of detectors. The detector records how long it took for the ray to reach it as well as the energy it deposited. Distance is equal to velocity*change in time. In respect to a pair of gamma rays, the change in time and velocity (assumed constant) are known but the exact length of the LOR, or distance, is needed as well.

Before the gamma rays arrive at the detectors, they interact inside the scintillator crystals coupled to them. A scintillator can trap a sole gamma ray and convert its energy into thousands of low-energy visible light photons whose collective energy is proportional to that of the ray—it is actually all of these photons that are hitting the detector, not the gamma ray. The location inside the crystal where the gamma ray was converted is known as the location of 'interaction'. Usually, the gamma ray's point of entry into the crystal will not be the same as its point of interaction. However, conventional clinical scanners treat the two points as one and the same, which produces an inaccurate LOR and as such the radiotracer's reconstructed location along it is wrong. It is easy to know which crystal a gamma ray interacted in: the crystal with the most energy at the correct time. It is difficult to know where along the length, or depth, of that crystal the interaction occurred. This lack of depth-of-interaction (DOI) information leads to geometric artifacts in the functional maps PET produces known as parallax errors. Decreases in these geometric artifacts translate to improved spatial resolution (Green et al., 2010) of small tumors (Son et al., 2014). Many groups have found ways to measure this depth of interaction, but the accuracy of these measurements is not high enough for clinical application. DOI resolution is the degree of uncertainty of a PET scanner's depth of interaction measurement, or how far off is the measured DOI value from the actual one.

Poor DOI resolution is related to the problem of poor spatial resolution (Green et al., 2010). In context of a PET scanner, spatial resolution indicates the smallest object that may be imaged clearly as well as refers to how well the scanner is able to differentiate between two objects. Spatial resolution can be represented by the point spread function (PSF). The full width at half maximum (FWHM) of this function is equal to the spatial resolution. The FWHM measures the "width" of a curved function, in which the width is not constant; it is an indicator of the statistical error of the data, similar to the standard deviation. Calculating this parameter is much easier than fitting a Gaussian function to raw data points. The narrower the PSF, the better the spatial resolution. The PSF depends on the gamma ray position across the field of view (Murata et al., 2016). As the source increases its distance away from the center of the scanner, the axial blur increases because the gamma rays have increased opportunity to interact with neighboring crystals instead of just the one directly across from it (Wiant et al., 2010). Fields such as small tumor imaging would be tremendously benefited by better spatial resolution.

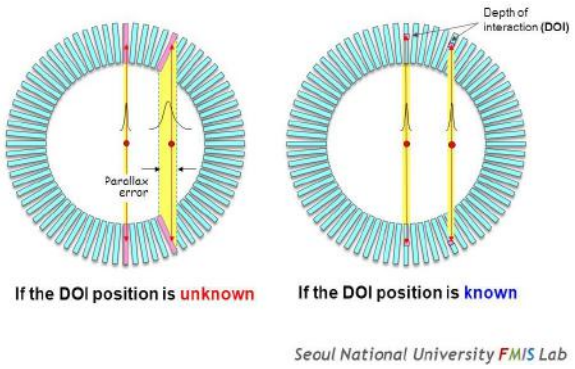

Figure 1: Parallax error in a PET scanner. The greater the width of the PSF, the lower the spatial resolution.

DOI resolution is primarily limited by the scintillation response, which includes the dynamics of the visible photons inside the scintillator crystal. The interaction point, or when the gamma ray is turned into visible light, is determined by a complex cascade process. If a gamma ray hits an electron in the valence band of a scintillator atom, the energy of the knocked off and therefore free electron is nearly equivalent to the ray it was hit by. This electron now has a massive amount of kinetic energy, most of which is released as heat as it collides into neighboring scintillator atoms. The rest is used to excite thousands of electrons in those atoms to the conduction band. If these electrons were to decay back down to the valence band, they would emit visible photons. However, the paths of these photons would be quickly terminated through reabsorption by other scintillator atoms. Thus, different energy states must be introduced into the otherwise forbidden gap between the valence and conduction band, usually via impurity addition. The electron still returns to the valence band, but it now goes by shorter steps because of these introduced states. The visible photons emitted have lower energies and longer wavelengths. The

photon does not have enough energy to excite other electrons and as a result can travel much farther. This facilitates light propagation as the photons are not reabsorbed by re-exciting their fellow scintillator atoms.

Partly the scintillation process is fundamentally limited due to the material itself. For example, relaxation of the electron-hole pairs into luminescent centers (created by impurities in the band gap) is a function of the material: those centers can be intrinsic or manufactured and their location varies depending on the lattice structure of the scintillator.

In our modules, 256 (16 by 16) Lutetium Yttrium Orthosilicate (LYSO) scintillation crystals are coupled to 64 (8 by 8) silicon photomultipliers (SiPM) in such a way that 4 crystals (2 x 2) are aligned with one SiPM. A reflector and a light guide are coupled to the top of the scintillator array. The visible light produced from a gamma ray interaction emits isotropically, or in all directions. As a result, 50% of the photons travel up and 50% travel down—the reflector ensures that after passing through the light guide, those upward-traveling photons do not escape the module. However, while some of that light is reflected back into the crystal it came from, the rest is shared between the neighboring crystals. The amount of light shared depends on the gamma ray's point of interaction (its DOI). For example, in respect to an interaction that occurs close to the detectors, majority of the downard traveling photons will reach the detector coupled to the crystal they originated from because the distance they must go is so small. As a result, the absorption probability by the crystal is low. However, the other half of the photons still must travel up a large portion of the scintillator, so the likelihood of their absorption is high and reduces the amount of photons that are shared with neighboring crystals. On the other hand, an interaction that occurs close to the light guide behaves in an opposite manner: more light is shared and reaches the neighboring detectors while less light reaches the parent detector. Because there is a different ratio of light shared to light not shared for each DOI, a unique distribution of charge arriving onto the detectors as whole is created. This distinctiveness allows for the comparison of one photon distribution to another as a way of determining the depth at which the gamma ray interacted.

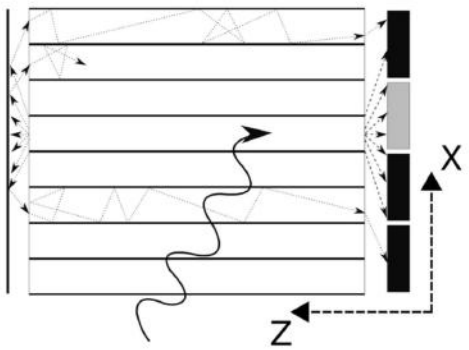

Figure 2. PET module set-up. From left to right: Reflector coupled to light coupled to scintillator array coupled to SiPM detectors.

Instead of one scintillator being coupled to one and only one detector, each scintillator, whose dimensions are smaller than those of the SiPMs, is coupled to 4 detectors. One scintillator takes up ¼ SiPM. One-to-one coupling, or one crystal per one SiPM is cost-inefficient and limits spatial resolution by the size of the scanner. This is so that when light get shared from one crystal to its neighbors, it will not hit the same SiPM that the downward traveling photons hit. Each SiPM detector produces an output when energy is deposited onto it. There will always be one detector that most of the energy was deposited on, but the directly adjacent peripheral detectors will also have some deposits of energy due to the light sharing. Spatial averaging of these outputs deduces the x and y coordinates of the point of interaction.

The variable 'w' represents the ratio between the charge (number of photons) collected by the pixel directly coupled to the crystal where the interaction occurred and the light collected the peripheral pixels. It is equal to $E_{maximum}/E_{total}$ where 'E' is energy (Pizzichemi et al., 2016). At different depths of interaction, this ratio will change. A high w value corresponds to low light sharing, and a low value to high sharing.

A uniform light guide, which is a flat rectangular piece of glass coupled on top of the crystal array, facilitates the light sharing by spreading the optical photons. However, the spread needs to be more confined because too much energy is being deposited onto the neighboring detectors that spatial averaging cannot be reliably completed. In addition, crystals at the edges of the module have less peripheral detectors so there is a lack of reference charge deposited, hindering spatial averaging which is essentially determining location based on the weighting of energy across all the detectors. This edge effect severely degrades image reconstruction. Specifically, there is severe resolution degradation at the edges of the module due to lack of reference information from at least one adjacent crystal. Gonzalez et al. has used horizontal and vertical light distribution projections—variations in which reveal the DOI. However, the same "truncation of light at crystal borders" interfered with DOI information at the module's edges and corners. This study examined the effects of scintillator surface treatment on light sharing between neighboring crystals, as this edge effect has been suggested to be reduced by lowering crystal reflectivity on the outermost lateral sides (Kaul et al., 2013).

Moreover, if DOI information is obtained by the sharing and redirection of scintillation light between multiple detectors, light dynamics within the scintillator limit DOI resolution. Total internal reflection (TIR) traps as much as 50% of optical photons inside the crystal. TIR occurs when a photon strikes a medium boundary at an angle larger than the critical angle, which is the angle of incidence above which total internal reflection occurs (Fernandez 2010). This is due to the polished lateral faces of the

crystals. It has been shown that inducing scatter reduces the amount of trapped light because it randomizes the direction of the photon by causing it to reflect at an angle not above the critical angle. By applying surface treatment, the optical symmetry of the scintillator can be disrupted by diffuse reflection.

Mechanically or chemically treating the sidewall surfaces, which as shown by Derenzo, Choong, and Moses are equivalent in effect, to make them rough can overcome TIR (Roncali and Cherry, 2013) and increase light output. Berg et al. showed via simulations that partial surface roughening caused a higher amount of photoelectrons to be reflected towards the detector. Considering the nature of isotropic photon emission, certain emitted photons that have not been trapped also cannot be used, or at least do not contribute to the leading edge of the SiPM signal, because they are located in escape cones created by the rectangular prism-shaped crystal—surface treatment can help break some of the photons in these cones free (Birks, 1995).

Some amount of TIR is necessary to actually have depth-dependent information (Blackberg et al.) because otherwise all photon paths would be extremely random and the amount of light shared would not vary according to DOI. However, at the top of the crystals there is already too much light output because any output is exacerbated by the light guide, which cannot be simply removed because it is necessary for light sharing.

By implementing partial surface roughening, or a combination of polished and depolished (rough) regions on the crystals' lateral faces, directional control of light can be achieved. This provides the peripheral pixels with enough charge so that there is a contrast with the main signal (from the detector the scintillator the event occured in is coupled to) but not so much so that the signals of all the detectors are too similar to average out to the correct crystal. Here, this type of surface treatment was used in conjunction with a uniform light guide.

Methods:

Simulation Methods: When the average 'w' value vs DOI is plotted, the DOI resolution can be found (Pizzichemi et al., 2016) by fitting a linear correlation between the two values and a slope is found. Once that slope has been found, it can be plugged in as a constant when finding the DOI resolution. Monte Carlo ray-tracing software TracePro was used to model the light propagation in a PET module. First, a rough surface had to be simulated that accurately represented an actual crystal that had been mechanically roughened. Crystals are depolished isotropically, or uniformly.

A 10 mm long depolished scintillator crystal was scanned by a one-dimensional stylus profilometer to characterize its roughness. Surface roughness regards the variations in the height of a surface as a function of scanning length, relative to a reference plane.

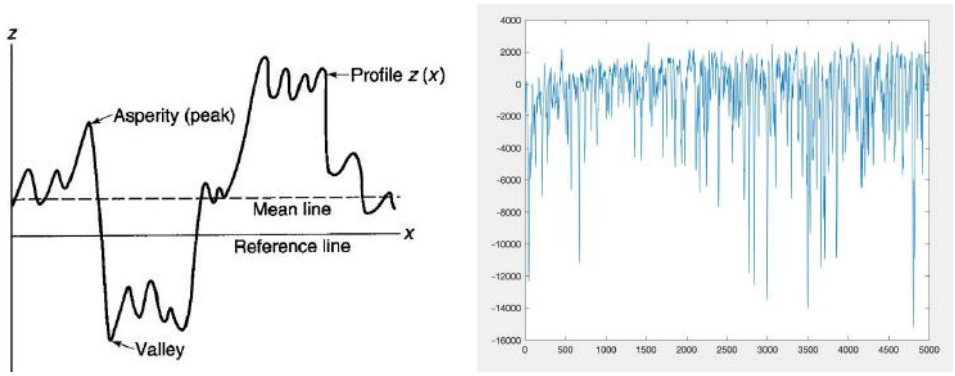

Figures 3-4. Left: The output of 1D stylus profilometer. Right: The experimental 1D scan used in this work. The x-axis is distance in microns transverse and the y-axis is the surface height.

A commonly used roughness parameter is the standard deviation of the surface height, or its root mean square (RMS) deviation. This parameter is a function of the mean height of the surface, as the roughness is characterized by the height deviations from the mean plane. The limitation of RMS analysis is that two surfaces can be qualitatively very different but still have the same RMS value. Those hypothetical surfaces are still different horizontally—the net deviation from the mean plane may be the same, but information regarding where along the mean plane the peaks and valleys occur is not factored in–critical as light will scatter differently depending on what that information says.

Power spectral density (PSD) analysis also characterizes surface roughness but does take into account this lateral information, or where these peaks and valleys start and end. If the surface height is rising, the profilometer will form a peak. If the surface height is falling, a valley. While RMS is related to PSD, they are not the same parameter. The RMS is the area under a 1D PSD curve and the volume under a 2D PSD topography map. A one-dimensional power spectral density is a function defined in frequency space while a two-dimensional PSD is a surface in frequency space.

All signals are the sums of various sine curves of varying frequencies. When a signal is deconstructed into a sum of sines, which frequencies make up the original signal can be seen. A Fourier transform performs this deconstruction by decomposing the surface into spatial wavelengths. A PSD represents the average contribution of each frequency to the total power. FFT in MatLab “takes a digital signal containing a certain number of samples and expresses it as the weighted sum of an equivalent number of frequencies.” Some frequencies contribute more to the overall signal than others. Spatial domain refers to the height of surface over a well-defined domain in space (a waveform) whereas the

frequency domain refers to the amplitude of sinusoids that compose the waveform in that same domain.

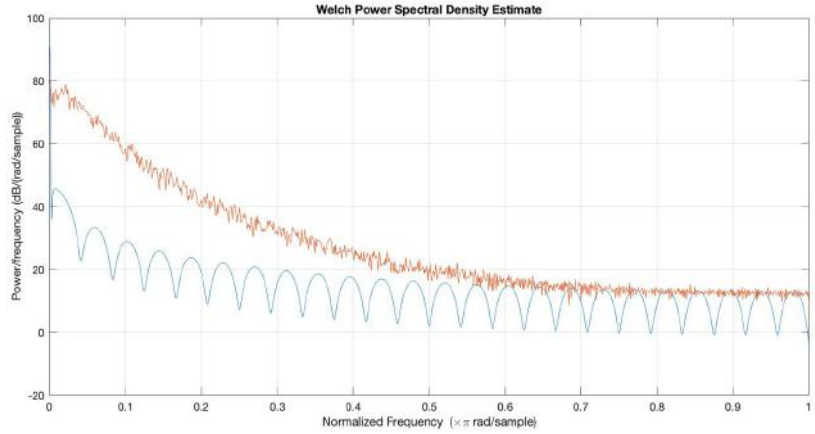

Figure 5. Orange: PSD derived from 1D profilometer scan. Blue: 100 PSDs all from different portions of the line scan stitched together.

The PSDs must be averaged in order to be accurate. The 1D PSD is "exceedingly noisy and non-reproducible" (Khan et al., 2004). These surfaces have random roughening, so the average of PSDs from different lengths of the sample provide a truer representation of surface variation. As such, a long profile can be subdivided into smaller profiles by breaking up the domain. The PSD can be found of each of these segments, and then averaged together. Because ideally surface roughening should be uniform, this average value does not make any assumptions about the surface.

In order to derive the 1D PSD from a line scan, the ABC/K-correlation model was used. An experimentally derived PSD from profilometer data can be fit using this model, which returns three parameters (A, B, and C) that describe the fit of the model.

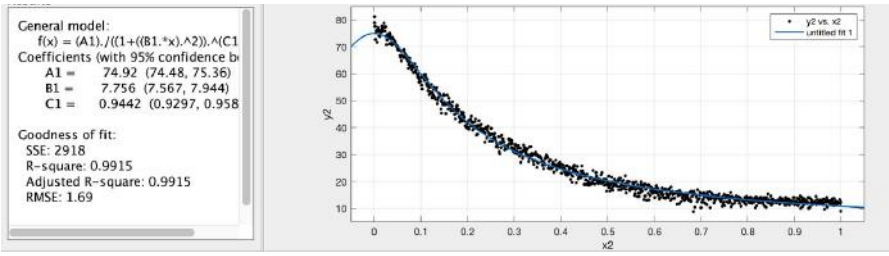

Figure 6. Experimental PSD fitted with ABC model.

The 1D PSD must be converted to a 2D PSD that represents the contribution of each signal that makes up a topographic map. In order to derive the 2D PSD from the 1D, A_2 must be found; it is proportional to the 'A' value found used the ABC model and found by the following equation.

$$A_2 = A_1 \frac{B\,\Gamma[(C+1)/2]}{2\sqrt{\pi}\,\Gamma(c/2)}$$

The power spectral density of a 2D surface is proportional to its bi-directional distribution function (BRDF), which uses the PSD's power distribution and predicts how light at a given incident angle will be scattered off a rough surface. In other words, it is the ratio of the quantity of light reflected in a direction (radiance) to the quantity of light arrived from a direction (irradiance). Given a light ray's incoming direction and the amount of light reflected in a direction, the BRDF outputs an intensity. For example, incoming light is perfectly reflected off of a perfect mirror, so the angle of incidence is equal to the angle of reflectance.

$$BRDF = \frac{16\pi^2}{\lambda^2}\cos\theta_i \cos\theta_s Q\, PSD(f)$$

As shown by the equation for BRDF on the right, it is a function of the incident angle of light, the scattered light, and the surface's PSD.

In order to derive the BRDF from the 2D PSD the Modeled Integrated Scatter Tool (MIST) software was used. The A_2, B, and C parameters were used and integration of the resulting reflectance distribution was calculated. 'Scatter Beta', which is equal to the $\sin(\theta_{incident})$ minus $\sin(\theta_{scattered})$, is the independent angular variable the BRDF is a function of; this parameter describes how much the scattered light deviated from the incident beam of light—this deviation changes depending on the surface roughness. Once a set of BRDF values were calculated for a set of incident angles, that data was input into TracePro to create a surface property that could be applied to any region of the simulated crystal.

Experimental Methods:

To experimentally confirm the poor DOI resolution of modules without any depolishing, radioactive point source Sodium 22 was placed between a module and a reference crystal. This set-up took advantage of the two antiparallel photons emitted as the point source decayed; the pairs of photons that were in true coincidence were selected and matched with the energy deposited at the time they were detected. The source could be moved up and down so the resolution of different depths of interaction measurements could be tested. Since the gamma ray interaction point's z-coordinate is directly related to the variable 'w', which in turn is directly related to the DOI resolution we can test how good our resolution is by performing tests at different values of z. Crystals were tested at 5 different depth for DOI resolution. 'W', or degree of light shared, is related to the DOI value of a gamma ray interaction because the amount of light shared is a function of this interaction. As such, the point source was emitting hundreds of gamma rays per second. For each of these hundreds of gamma ray interactions, the outputs of all 64 SiPM signals are being recorded, which were then used to calculate 'w'. Hundreds of 'w' values will be generated for each DOI value, and while they should be similar, they will not be the exact same. All of these 'w' values were plotted against DOI. Naturally, these values clustered around a certain value.

These clusters of points were fitted with a Gaussian curve. The FWHM of this curve was said to be the DOI resolution. The narrower the width of the curves, the less variability among all the ‘w’ values. Lower variability means that the crystals were treated in such a way that consistent ‘w’ values were being produced. In a real life scenario, z of course would not be known but if these crystals were to be used in a scanner, reconstruction of radionuclide location could be said with certainty equal to the FWHM of those earlier described curves.

The z coordinate of the gamma ray interaction is known, and w is derived. In our experimental setup, the depths along the length of the crystal were known. However, they were also reconstructed using the methods described above, using the ‘w’ distributions. How far off these two values are determined the DOI resolution.The source was placed inside a 1-inch thick lead collimator and the whole set-up inside a temperature-controlled chamber as the readout electronics attached to the detectors are sensitive to temperature change.

The outputs of the SiPM detectors were used to calculate ‘w’, as they record how much energy from visible light was deposited onto them as well as what time it was deposited. Time-over-threshold analysis, performed by the readout electronics coupled to the detectors, derives the energy deposited from the widths of the output pulses from the SiPMs. Raw data includes the 64 energy deposits from the 64 SiPMs. Time-over-threshold is a method commonly used for signal processing of SiPM analogues. Two independent threshold values are used: the timestamp of the event and the length of the pulse. Each of those two values can be discreetly extracted from all of the 64 channels. These values are then digitized and averaged. A ray that hit a corner crystal will not produce outputs in another corner of the module because light is not shared from that corner crystal all the way there. Thus the SiPM output indicate zero energy deposition. The top five highest SiPMs outputs that occured at relatively the same time are averaged to find both the actual crystal the ray hit as well as the ‘w’ value.

Results and Discussion:

Optimal surface treatment aims to increase light output at the bottom of the crystal by decreasing total internal reflection, while slightly decreasing light output at the top. There is nonuniformity of TIR, as shown by Spanoudaki and Levin, depending on the length of the crystal. In longer, polished crystals the light output is less. A long crystal will delay many of the photons due to lots of bouncing around in the crystal, thus increasing absorption probability. Ideal surface treatment decreases TIR, but allows modules to still use long crystals, which are essential because the length is why gamma rays are trapped so effectively.

The aim of such treatment is to expand the range of 'w' as a function of DOI values, by increasing the highest 'w' value and decreasing the smallest one. Since DOI resolution is the FWHM of the curves that fit thousands of these 'w' values at specific DOI values, the more those curves blur into each other (Figure 19), it is with less certainty one can say a certain 'w' value indicates a certain DOI. Thus, if the range is expanded, the curves are more separated. Out of all the various combinations of polished and unpolished lateral surfaces, when the bottom 11 mm of one lateral face was roughened, the range of 'w' values was the most wide (Figure 15). The dimensions of each crystal are 1.4 mm x 1.4 mm x 20 mm. The benefits of optimal partial surface roughening would not have been achieved if not used in conjunction with a uniform light guide (Figures 8-10).

By roughening approximately 50% of one lateral face, light output from the bottom of the crystal was increased and as a result more photons reached the detector, increasing the numerator ($E_{maximum}$) of 'w'. Likewise, at the top of the crystal, light is already being shared so there is no need to increase light output there. Most likely, treating only one side also helped confine light sharing at the top of the crystal. Because the net redirection of the photons was shown to be downward, the likelihood that the photons in the middle of the crystal will travel downard increased, slightly decreasing the amount of photons shared at the top. Enough photons are still shared, because of the light guide, just lesser amount. Therefore, spatial averaging of the energy signals can still be performed, but no longer are the signals from each signal too similar to deduce detector was coupled to the scintillator the gamma ray hit. Overall, the light that arrived onto the detectors was less spread out, and of more variant intensity. Again, if the detector outputs are significantly different, when energy weighting is performed to see which point the most energy is localized, that point will be more accurate.

Just like fully polished sidewalls resulted in inconsistent 'w' values, so did the fully roughened crystals (Figures 13-14).The amount of light output has to be delicately balanced—the fully depolished crystals had too much light output at every point along the length of the crystal. As a result, the depth-dependent information is lost because the light sharing distribution is no longer proportional to depth. There is no directional control of light.

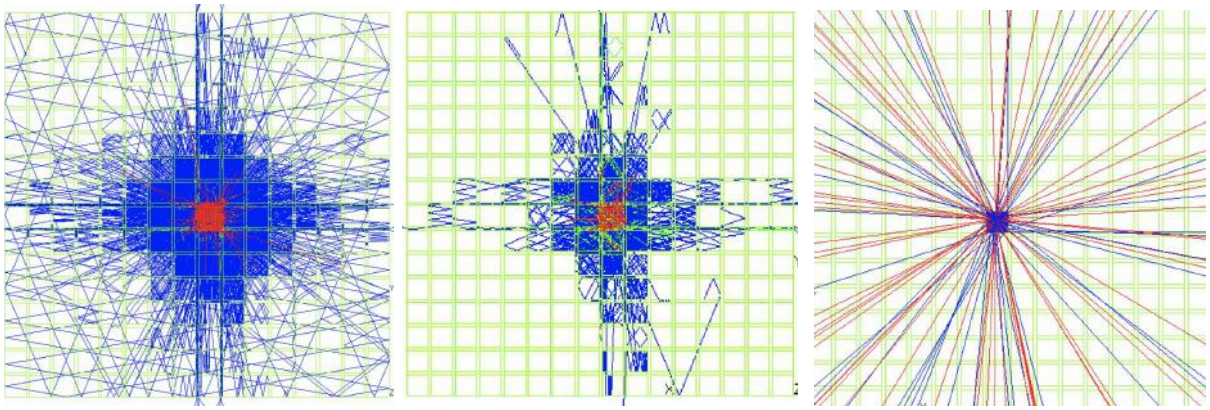

Figures 8-10. Left: Polished sidewalls and light guide; Middle: Partial surface roughening and light guide; Right: Polished sidewalls with no light guide.

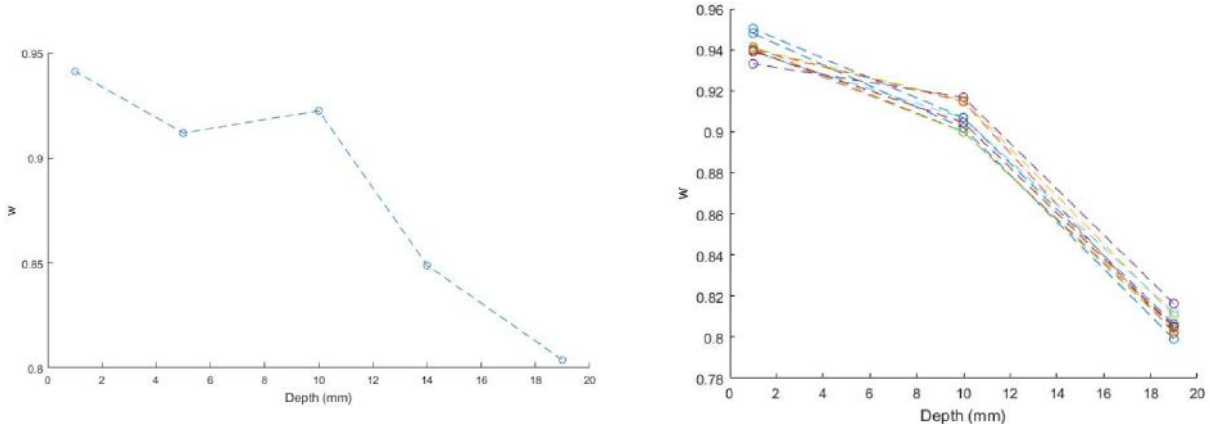

Figures 11-12. Simulation results for polished crystals in conjunction with a uniform light guide. The average ‘w’ value is plotted against depth of interaction. Right: average of 1000 trials. Left: 5 trials.

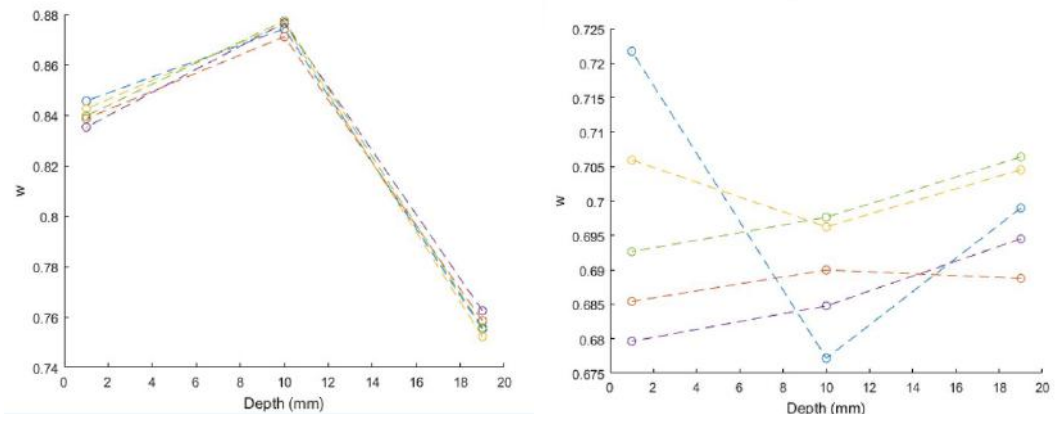

Figures 13-14. Simulation results for fully roughened lateral faces.

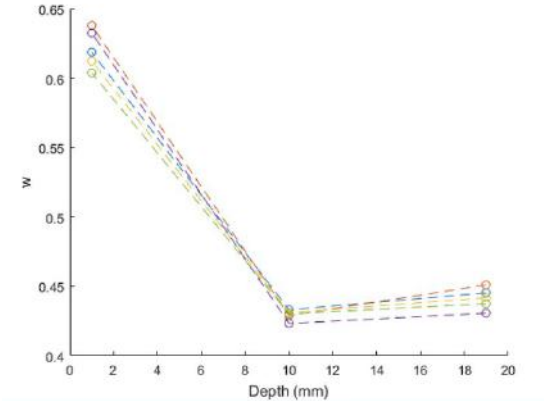

Figure 15. Simulation results for roughening applied to bottom 11 mm of one lateral face. The highest range of w is shown.

The effect of TIR is exacerbated by the very high index of refraction scintillation crystals have. When the light guide's index of refraction was matched to that of the crystal, regardless of surface roughening, the light output at both ends increased because the transition from one material to the other was made more seamless.

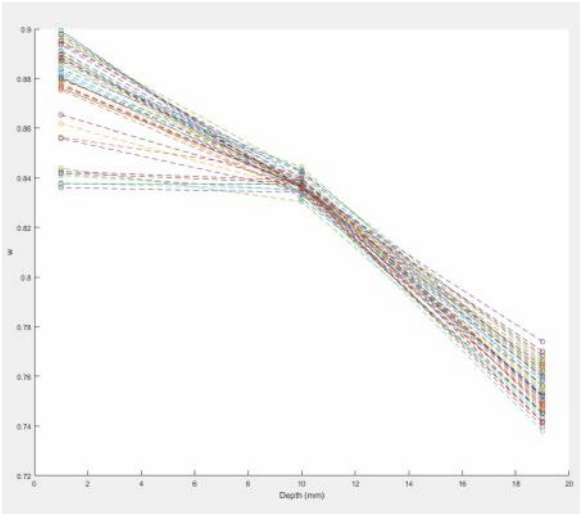

Figure 16. 'W' vs. DOI for index of refraction matching between crystal and detector.

Crystal separation was also improved because of this (Figures 17-18), most likely because of the increase in light output as less photons are undergoing less total internal reflection, in alignment with Berg et al. As shown in figure 18, the edge effect is substantially decreased due to enhance light output—almost all of the crystals ate the edge of the module have the same amount of energy deposited as those in the middle. Flood histograms are two dimensional graphs created by completely and evenly irradiating the detector module (Lau et al., 2012) with gamma rays. The x and y positions of the interaction as calculated are arbitrary values, meaning they cannot be translated to an actual location on the detector. Thus, the x and y values have to be calibrated to scale within the module's real dimensions.

However, the two-dimensional positions of thousands of events are calculated. As such, the positions will not perfectly coincide, but they will still be proximal to one another, forming clusters. All of these coordinates are plotted, and the clusters seen when this is done each represent the position of one detector element. However, these clusters do not align with each other linearly, even though the elements they represent do. This is due to the distribution of light not aligned with the actual location of the detector elements. The centroid of each cluster is found and a range of accepted values (depending on photopeak) above and below the centroid value is made. Then, during a later acquisition of events, an event can be assigned into its correct element based on its coordinates; those coordinates are assigned to a range. The irradiation is done to the side of the array, which is in a light-tight box. Obviously, it is important for the detector elements to be qualitatively distinct from one another in these maps because an event cannot be detected between the elements, so if a point does show up between the elements, something is wrong.

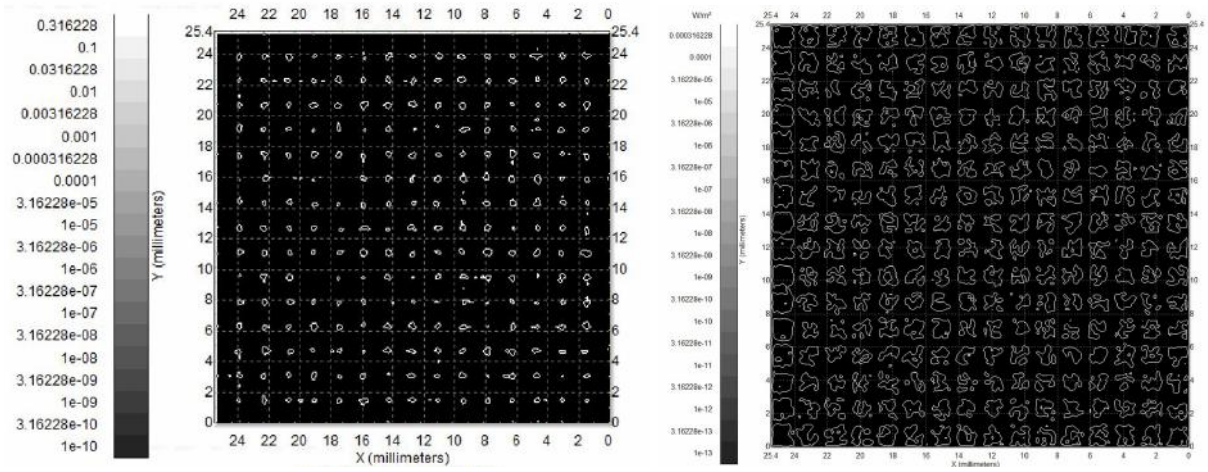

Figures 17-18. Left: Log-scale polished flood histogram. Right: Log-scale partially depolished flood histogram.

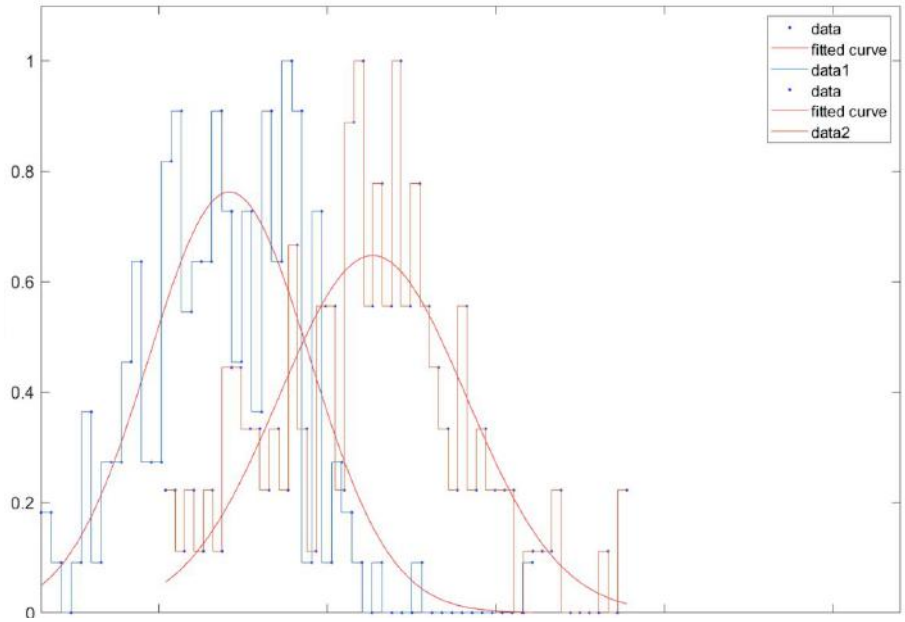

Figure 19. Experimental test for uniform light guide and crystals with no surface roughening. Two DOIs are represented by the two curves. The y-axis represents the values of 'w'. The peaks blur together, a sign of low DOI resolution.

As with any simulation, certain assumptions are made. The intrinsic scintillator response is not taken into account. Ideally, the production of photons would be extremely fast, so the time they were emitted is very close to the time they were detected. Excitons decay to different levels, emitting photons as they do. If they decay to really low levels, the process is longer. Once those photons have been produced, there is a transit time from their emission point to the photodetector, which was not accounted for in my simulation.

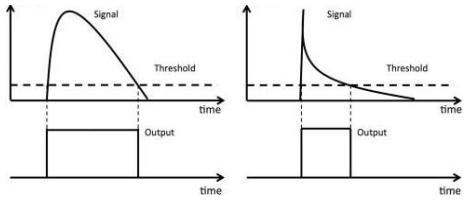

Figure 20. Output pulse of an SiPM. The graph on the right shows that the faster the photons reach the detector, the less variance the output has.

Inherently within scintillation statistics is a timing uncertainty (Figure 20) due to the photon transit time. Because the travel time of each optical photon is not instantaneous or unanimous, a lower bound is set to achievable timing resolution. The scintillation light produced from a gamma ray event emits in all directions, or isotropically. As such, part of the photon flux travels directly towards the photodetectors, while another part travels up the crystals towards the reflector. The latter fraction of photons will eventually reach the detector as well as the reflector ensures they do not escape into the air,

but they will arrive at much later time. It is important to extract the timestamp of those first photons because they are the most accurate representation of the interaction event, as theoretically without timing jitter of the photodetector and the scintillator response, the photons would travel much faster and much more uniformly (and creating a much smaller time distribution). Those initial photons are the ones that did not have to face as much jitter or sidewall bouncing; if they did, they would not have arrived first. The number of initial photons should be maximized because just one photon may not trigger an avalanche in the detector. Timing pick-off, or when time information is extracted from the pulse: the triggering of an SiPM output should be commenced at the first few detected photons (Yeom et al., 2013).

Moreover, fully depolished crystals have been shown to have a 700 picosecond transit time whereas generated inside polished crystals had a maximum transit time of 160 ps. More tests are needed to determine if improvements in DOI resolution degrades timing resolution. As important as DOI resolution is timing resolution which is affected by how long it takes for a photon to reach the detector from point of interaction. Only gamma rays in true coincidence, that is having arrived at the detector at around the same time. If one ray of a pair of gamma rays reaches significantly earlier than another due to delays caused scintillator finish, their energy deposits may be rejected because they "have no pair", even if they do. Surface treatment having a negative effect on timing resolution contradicts Jatekos et al.'s work that showed helping otherwise trapped photons find their way out of the crystal can improve timing and energy resolution as well. These conflicting reports would need to be resolved through further tests.

By selectively inducing TIR, the amount of light output at different points along the crystal was optimized and thereby so was DOI resolution. Surface treatment alone cannot achieve this; the partial treatment only led to better crystal separation, decrease in the edge effect, and range expansion of 'w' when it was used concurrently with a uniform light guide. In addition, the net light distribution at any of the depths was more confined, even though TIR was decreased. This is alignment with the notion of favorable light output—favorable does not necessarily mean more. Different amounts of light output are needed respective to the different depths along the crystal. A critical limitation was that Compton scattering was not taken into account in the simulations but did play a role in the experimental result. Compton Scattered gamma rays that do not have a pair associated with them is a phenomenon of radionuclide decay. These rays can create interactions inside the crystals as well, which can slightly skew the data because only data from a pair of rays should be included—only a pair can create a line of response. This is inevitable when using lead collimation, so proper post-processing should be done to filter out the data produced by Compton scatter. While the improved DOI resolution can extrapolated to better spatial resolution, more research in the future needs to be done evaluating how partial surface

roughening affects timing resolution, as this is the second parameter limiting the capability of PET scanners.

Bibliography:

Fernandez, P. D. (2010). Simulation of the light detection for the optimization of CALIFA crystals.

Green, M. V., Ostrow, H. G., Seidel, J., & Pomper, M. G. (2010). Experimental Evaluation of Depth-of-Interaction Correction in a Small-Animal Positron Emission Tomography Scanner. *Molecular Imaging, 9(6)*.

Khan, G. S., Sarepaka R. G. V., Chattopadhyay, K. D., Jain, P. K., & Bajpai, R. P. (2004). Characterization of nanoscale roughness in single point diamond turned optical surfaces using power spectral density analysis. *Indian Journal of Engineering & Materials Sciences, 11.*

Lecoq P. (2012). New Approaches to Improve Timing Resolution in Scintillators. *IEEE Transactions on Nuclear Science*, *59*:2313–2318.

Moses, W.W., & Derenzo, S.E. (1994). Design studies for a PET detector module using a PIN photodiode to measure depth of interaction. *IEEE Transactions on Nuclear Science*, *41.*

Pizzichemi, M., Stringhini, G., Niknejad, T., Liu, Z., Lecoq, P., Tavernier, S., Varela, J.,…Auffray, E. (2016). A new method for depth of interaction determination in PET detectors. *Physics in Medicine and Biology, 61*.

Roncali, E., & Cherry, S. R. (2013). Simulation of light transport in scintillators based on 3D characterization of crystal surfaces. *Physics in Medicine and Biology, 58(7)*.

Spanoudaki, V. C., & Levin, C. S. (2011). Investigating the temporal resolution limits of scintillation detection from pixellated elements: comparison between experiment and simulation. *Physics in Medicine and Biology, 56.*